doi:10.3772/j.issn.1006-6748.2023.01.010

Simulation analysis of wear characteristics of connecting rod bearing bush based on improved mixed lubrication model①

GAO Yunduan(高云端)*, WANG Zijia**, TIAN Ye*, HUANG Yan*, ZHANG Jinjie②***
(*Beijing Changcheng Aeronautic Measurement and Control Technology Research Institute, Beijing 100176, P. R. China)
(**State Key Laboratory of Tribology, Tsinghua University, Beijing 100084, P. R. China)
(***Beijing Key Laboratory of Health Monitoring and Self-Healing of High-end Mechanical Equipment, Beijing University of Chemical Technology, Beijing 100029, P. R. China)

Abstract

The failure rate of crankpin bearing bush of diesel engine under complex working conditions such as high temperature, dynamic load and variable speed is high. After serious wear, it is easy to deteriorate the stress state of connecting rod body and connecting rod bolt, resulting in serious accidents such as connecting rod fracture and body damage. Based on the mixed lubrication characteristics of connecting rod big endbearing shell of diesel engine under high explosion pressure impact load, an improved mixed lubrication mechanism model is established, which considers the influence of viscoelastic micro deformation of bearing bush material, integrates the full film lubrication model and dry friction model, couples dynamic equation of connecting rod. Then the actual lubrication state of big end bearing shell is simulated numerically. Further, the correctness of the theoretical research results is verified by fault simulation experiments. The results show that the high-frequency impact signal with fixed angle domain characteristics will be generated after the serious wear of bearing bush and the deterioration of lubrication state. The fault feature capture and alarm can be realized through the condition monitoring system, which can be applied to the fault monitoring of connecting rod bearing bush of diesel engine in the future.

Key words: mixed lubrication model, connecting rod bearing bush, wear, fault feature, condition monitoring

0 Introduction

Medium high-speed and high-power diesel engine is the core power equipment of military and civilian ships. It has been heavily dependent on foreign technology licensing production for a long time, and its independent research and development and operation and maintenance management ability is weak. With the increasing complexity of marine diesel engine system and the continuous improvement of integration and intelligence, the failure rate of key components of marine diesel engine continues to rise under harsh environments such as high temperature, high speed, strong corrosion, strong impact and variable working conditions, as well as malignant faults such as connecting rod fracture, connecting rod bolt fracture and valve fracture occur frequently[1-2]. It seriously endangers the safe and reliable navigation of military and civilian ships.

Medium and high-speed, high-power marine diesel engines have the characteristics of many cylinders, large cylinder diameter, high explosion pressure and complex structure. Under the combined action of high explosion pressure combustion impact force, reciprocating inertia force and rotating centrifugal force, their crank connecting rod mechanism bears alternating and strong impact loads for a long time. Their common variable speed and variable load conditions superimpose combustion impact in the cylinder, resulting in complex lubrication conditions and frequent faults of connecting rod bearings, such as wear, cracks loose bushing. The wear of connecting rod bearing will cause the increase of fitting clearance, lubrication failure, abnormal impact vibration and shear stress, deteriorate the stress state of connecting rod body and connecting rod bolt, and easily cause malignant accidents such as connecting rod bolt fracture, connecting rod fracture, and even serious damage to the body[3]. Therefore, accord-

① Supported by the National Natural Science Foundation of China (No. 52101343) and the Aeronautical Science Foundation (No. 201834S9002).
② To whom correspondence should be addressed. E-mail: zjj87427@163.com.
Received on May 9, 2022

ing to the structure, lubrication and operation characteristics of marine diesel engine connecting rod bearing, it is particularly urgent to carry out in-depth research on the fault mechanism of connecting rod bearing, so as to monitor and diagnose the fault and ensure the safe and stable operation of the unit.

In recent years, researchers have strengthened their investment in the study of diesel engine fault mechanism. Daniel and Cavalca[4] established a full film lubrication state model for the small end bearing of connecting rod, which is suitable for the small eccentricity of piston pin. For the connecting rod big end bearing, Chen and Ranadall[5] adopted the lubrication model of infinite short sliding bearing based on the local coordinate system, and obtained the dynamic response of connecting rod bearing under the condition of full film lubrication. Haneef et al.[6] coupled the rough peak contact model to simulate the most widely existing mixed lubrication state in connecting rod bearings, and established the lubrication state transition mechanism based on the film thickness ratio. Hou and Du[7] calculated the stress time load of diesel engine bearing components based on multi-body dynamics theory, and completed the surface vibration analysis of engine block structure by finite element method. Yuan et al.[8] studied the fault mechanism of diesel engine timing gear fracture by computer simulation combined with metallographic analysis of metal materials. Bi et al.[9] established the thermal elasto hydrodynamic lubrication (TEHL) model of connecting rod small end bearing and analyzed the effects of bearing clearance and surface roughness on wear characteristics under the influence of heat load. The existing research on bearing lubrication and wear generally ignores the micro deformation time and rough peak contact effect of bearing materials. Assuming that the bearing bush material is completely elastic, the quantitative relationship between local micro deformation and wear evolution of bearing materials cannot be established, and it is difficult to accurately analyze the generation and change law of weak impact signal of early wear of connecting rod bearing under strong impact load and variable working conditions.

In recent years, scholars have carried out research on the viscoelastic effect of solid materials. Scaraggi and Persson[10] proposed a viscoelastic hydrodynamic lubrication (VEHL) model suitable for steady-state point contact or line contact, coupled Boussinesq's half space deformation theory[11-12] and viscoelastic constitutive equation to correct the calculated value of steady-state deformation. He et al.[13] further studied the effect of temperature on viscoelastic deformation on the basis of VEHL model, and proposed a new thermal viscoelastic hydrodynamic lubrication model. It should be pointed out that these viscoelastic hydrodynamic lubrication models are suitable for point contact or line contact lubrication forms, such as rolling bearing and gear meshing, and have poor adaptability to sliding bearing. According to the viscoelastic deformation characteristics of dynamically loaded sliding bearings, a time-series related deformation equation is proposed, which can reveal the mechanism of alternating transient and time-delay deformation and coupling effect of lubrication flow field boundary[14].

Based on the existing achievements, this paper takes the connecting rod big end bush of four stroke diesel engine as the research object, establishes the time series related mixed viscoelastic hydrodynamic lubrication model, considers the influence of viscoelastic micro deformation of bearing bush material, and constructs the full lubrication state analysis model of connecting rod bearing bush by integrating the full film lubrication model and dry friction model. Furthermore, the impact characteristics of the connecting rod bearing bush under the actual lubrication state and wear state are numerically simulated by coupling the connecting rod dynamic equation. The correctness of the theoretical research results is verified experimentally by using the diesel engine fault simulation test-bed. The simulation and experimental results show that the high-frequency impact signal with fixed angle domain characteristics will be generated after the bearing bush is seriously worn and the lubrication state is degraded. The research results of this paper have a positive role in promoting the research on the fault mechanism and diagnosis method of connecting rod bearing bush of diesel engine.

1 Construction of full lubrication analysis model for connecting rod bearing bush

Previous studies have proved that during the operation of piston engines, the lubrication state of the connecting rod bearing bush changes periodically and constantly changes in three states, including full-film lubrication state, mixed lubrication state and dry friction state, as shown in Fig. 1. These three lubrication states can be distinguished by the minimum film thickness ratio[14]. In this paper, different lubrication models are used to calculate the bearing resultant forces under three lubrication states.

1.1 Mixed lubrication state model

When the minimum film thickness ratio $0 \leqslant H_{\min} \leqslant 3$, namely eccentricity ratio $1 \geqslant \varepsilon \geqslant 1 - 3\sigma / c$,

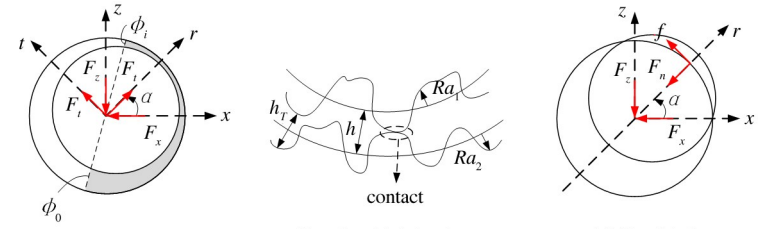

(a) Full-film lubrication (b) Mixed lubrication (c) Dry friction

Fig. 1 Schematic diagram of lubrication state

bearing bush is in mixed lubrication state. In this state, local oil film thickness, surface roughness and deformation belong to the same order of magnitude, so there is both oil film lubrication and microscopic rough contact. Deformation and rough contact affect the oil film thickness and thus the oil film pressure.

(1) Calculation equation of deformation and oil film thickness. The time-series associated deformation equation considering the viscoelasticity of bearing bush material can be written as

$$\begin{cases} \delta_L(x', y', \Delta t)\mid_t = \delta_L(x', y', t)\left[e^{(-\Delta t/\tau_b)} - 1\right] \\ \qquad + \delta_L^{p(x', y', t)}(x', y', \infty)\left[1 - e^{(-\Delta t/\tau_b)}\right] \\ \delta(x', y', t + \Delta t) = \delta_T(x', y', t + \Delta t) \\ \qquad + \sum_{i=1}^{t/\Delta t}\delta_L(x', y', \Delta t)\mid_i \end{cases} \tag{1}$$

where, x and y respectively represent the two radial directions where the bearing bush sections are perpendicular to each other, $\delta_L(x', y', \Delta t)\mid_t$ is the unit delay deformation of bearing bush, $\delta_L(x', y', t)$ is the cumulative delay deformation, $\delta_L^{p(x', y', t)}(x', y', \infty)$ is the complete time-delay deformation produced by the corresponding time-elastic modulus E_L under the current oil film pressure $p(x', y', t)$, $\delta_T(x', y', t + \Delta t)$ is the transient deformation corresponding to the transient elastic modulus E_T at the next time, $\delta(x', y', t + \Delta t)$ is the total deformation of superimposed transient and delay deformation.

Therefore, the oil film thickness calculation equation including deformation and roughness correction can be written as

$$h_0(x', t) = c + e(t)\cos\left(\frac{x'}{R_b}\right),\ \frac{x'}{R_b} = \varphi \in [0, 2\pi] \tag{2}$$

$$h(x', y', t) = h_0(x', t) + \delta(x', y', t) \tag{3}$$

$$\overline{h_T} = E(h_T) = \int_{-h}^{\infty}(h + Ra)f(Ra)\,\mathrm{d}Ra \tag{4}$$

where, $h_0(x', t)$ is nominal oil film thickness (not considering bearing deformation), $h(x', y', t)$ is the oil film thickness taking into account of bearing bush deformation, $\overline{h_T}$ is the average oil film thickness, R_b is the bearing radius, c is the bearing radius clearance, e is eccentric distance, $Ra = Ra_1 + Ra_2$ is combined roughness, $f(Ra)$ is the probability density function of Ra.

(2) Oil film pressure control equation. The oil film pressure control equation considering surface roughness is the average Reynolds equation proposed by Patir and Cheng[15].

$$\frac{\partial}{\partial x'}\left(\psi_x\frac{h^3}{12\mu}\frac{\partial p}{\partial x'}\right) + \frac{\partial}{\partial y'}\left(\psi_y\frac{h^3}{12\mu}\frac{\partial p}{\partial y'}\right) = \frac{U_1 + U_2}{2}\frac{\partial\overline{h_T}}{\partial x'} + \frac{U_1 - U_2}{2}\sigma\frac{\partial\psi_s}{\partial x'} + \frac{\partial\overline{h_T}}{\partial t} \tag{5}$$

where, ψ_x and ψ_y are pressure flow factor, ψ_s is shear flow factor. All of them can be calculated by using Patir and Cheng's empirical formula based on numerical simulation results.

1.2 Full-film lubrication state model

When the minimum film thickness ratio $H_{\min} > 3$, namely eccentricity ratio $\varepsilon < 1 - 3\sigma/c$, bearing bush is in full-film lubrication state. The thickness of oil film is larger than that of film pressure, and the influence of surface roughness, deformation and viscosity effect of oil can be ignored. Ocvirk[16] has derived the analytical solution of oil film pressure of infinitely short plain bearings based on Reynolds equation. The model is used to calculate the oil film pressure of bearing bush under the condition of full-film lubrication, and the analytical function of the film pressure can be expressed as

$$p(\phi, y') = \frac{6\mu c}{h^3}\left[\dot{\varepsilon}\cos\phi + \varepsilon(\dot{\alpha} - \bar{\omega})\sin\phi\right]\left(y'^2 - \frac{1}{4}L^2\right) \tag{6}$$

where, ϕ is the circumferential angle of the rotating coordinate system of the big end bearing shell, $\bar{\omega}$ is the relative speed between the crank journal and the big end bearing shell, h is the nominal oil film thickness, and their calculation formulas are as follows.

$$\begin{cases} h(\phi) = 1 + \varepsilon\cos\phi \\ \bar{\omega} = \dot{\theta} - \dot{\varphi} \end{cases} \tag{7}$$

The model has two boundary conditions. The first boundary condition considers that the oil film is com-

plete, so there is negative pressure. However, in practice, the liquid cannot withstand negative pressure, so there is a cavitation effect. The Gumbel boundary condition more reasonably considers the effective positive pressure oil film interval. The starting point ϕ_0 and the ending point ϕ_i of the interval can be calculated by

$$\begin{cases} \phi_0 = \arctan\left(\dfrac{-\varepsilon}{\dot{\varepsilon}(\dot{\alpha}-\bar{\omega}/2)}\right) \\ \phi_i = \phi_0 + \pi \end{cases} \tag{8}$$

In addition, the interval starting angle φ_0 needs to be corrected, which can be expressed by

$$\phi_0 = \phi_0 + \pi, \text{ if } [\dot{\varepsilon}\sin\phi - \varepsilon(\dot{\alpha}-\bar{\omega}/2)\cos\phi] < 0 \tag{9}$$

1.3 Dry friction state model

When the minimum film thickness ratio $H_{\min} < 0$, namely the eccentricity ratio $\varepsilon > 1$, the big end bearing shell is in a dry friction state, and the crank journal and the big end bearing shell are in direct contact. In this section, the Hertzian elastic contact model modified by Lankarani and Nikravesh is used to calculate the normal contact force[17], which can be expressed as

$$\boldsymbol{F}_n = \left\{\frac{4\sqrt{\dfrac{R_b R_j}{R_b+R_j}}}{3\left[\left(\dfrac{1-v_b^2}{E_b}\right)+\left(\dfrac{1-v_j^2}{E_j}\right)\right]}\right\}\left[1+\frac{3(1-c_e)^2}{4}\frac{\dot{\delta}_{\text{in}}}{\dot{\delta}_{\text{in}}^{(-)}}\right]\boldsymbol{\delta}^{nc} \tag{10}$$

where, $\dot{\delta}_{\text{in}}$ is the contact penetration velocity, that is, the eccentric velocity $\dot{\varepsilon}$; $\dot{\delta}_{\text{in}}^{(-)}$ is the initial collision velocity and δ is the penetration amount $(\varepsilon c - c)$. For metal materials, the exponent nc is equal to 1.5, and the regression coefficient c_e is 0.9. In this state, the frictional force and frictional power consumption can be expressed as[18]

$$\begin{cases} \boldsymbol{f} = -c_f c_d \boldsymbol{F}_n \dfrac{R_b\bar{\omega}+c\varepsilon\dot{\alpha}}{|R_b\bar{\omega}+c\varepsilon\dot{\alpha}|} \\ P_o = |f(R_b\bar{\omega}+c\varepsilon\dot{\alpha})| \end{cases} \tag{11}$$

where, the friction coefficient c_f is 0.1 according to experience; $(R_b\bar{\omega}+c\varepsilon\dot{\alpha})$ is the tangential relative sliding speed of the contact point; c_d is the dynamic correction coefficient, and its value varies between 0 and 1 due to the influence of the relative sliding speed in the tangential direction, and it is 0.5 according to experience.

1.4 Bearing resultant force calculation model

In the state of oil lubrication, the oil film pressure is much greater than the friction force. Therefore, the bearing force is mainly composed of the oil film pressure and the rough contact pressure, and the influence of the friction force on the bearing resultant force is ignored. In the full film and mixed lubrication state, the calculation formula of bearing resultant force can be expressed as

$$\begin{cases} \boldsymbol{F}_r = \displaystyle\int_{\frac{-L}{2}}^{\frac{L}{2}}\int_{\phi_0}^{\phi_i} \boldsymbol{p}\cos\phi R_b \mathrm{d}\phi\mathrm{d}z' \\ \boldsymbol{F}_t = \displaystyle\int_{\frac{-L}{2}}^{\frac{L}{2}}\int_{\phi_0}^{\phi_i} \boldsymbol{p}\sin\phi R_b \mathrm{d}\phi\mathrm{d}z' \end{cases} \tag{12}$$

In the dry friction state, the resultant bearing force can be expressed as

$$\begin{cases} \boldsymbol{F}_r = -\boldsymbol{F}_n \\ \boldsymbol{F}_t = \boldsymbol{f} \end{cases} \tag{13}$$

where $\boldsymbol{F}_r$ and $\boldsymbol{F}_t$ are the components of the bearing resultant force along the local coordinate system rt, respectively.

Based on the coordinate transformation angle α, transform $\boldsymbol{F}_r$ and $\boldsymbol{F}_t$ into global coordinate system components, which can be expressed in matrix form as

$$\begin{bmatrix} \boldsymbol{F}_{xr} \\ \boldsymbol{F}_{zr} \end{bmatrix} = \begin{bmatrix} \cos\alpha & -\sin\alpha \\ \sin\alpha & \cos\alpha \end{bmatrix}\begin{bmatrix} \boldsymbol{F}_r \\ \boldsymbol{F}_t \end{bmatrix} \tag{14}$$

where, $\boldsymbol{F}_{xr}$ and $\boldsymbol{F}_{zr}$ are the bearing force components acting on the big end bearing shell, and the components $\boldsymbol{F}_{xc}$ and $\boldsymbol{F}_{zc}$ acting on the crank journal are the interaction forces with them.

To sum up, an analysis model of the full lubrication state of the big end bearing shell is constructed, and the film thickness ratio is used as the criterion to switch between different models, which corresponds to the calculation of bearing performance parameters in different lubrication states.

2 Construction of the dynamic model of the crank connecting rod mechanism considering the influence of lubrication

Due to the clearance at the big end bearing shell of the crankshaft connecting rod mechanism of diesel engine, it can be divided into two subsystems: piston connecting rod subsystem and crankshaft subsystem, as shown in Fig. 2. There is a pair of interaction forces between the two subsystems, that is, the bearing resultant force of the big end bearing shell, which can be obtained by the calculation model of the bearing resultant force mentioned above.

2.1 Piston connecting rod subsystem

Taking the friction pair in the subsystem as an ideal rotating pair, according to the Lagrangian energy method, the dynamic equation of the piston connecting rod subsystem can be written as

$$\begin{cases} \ddot{\varphi} = \dfrac{-(m_r + m_p)(F_{xr}L_c\cos\varphi + F_{zr}L_c\sin\varphi) + L_1 m_r \sin\varphi (L_1 m_r \dot{\varphi}^2 \cos\varphi + F_{zr} - F_g)}{-(L_1 m_r \sin\varphi)^2 + (I_r + L_1^2 m_r)(m_r + m_p)} \\ \ddot{z}_p = \dfrac{(I_r + L_1^2 m_r)(L_1 m_r \dot{\varphi}^2 \cos\varphi + F_{zr} - F_g) - L_1 m_r \sin\varphi (F_{xr}L_c\cos\varphi + F_{zr}L_c\sin\varphi)}{-(L_1 m_r \sin\varphi)^2 + (I_r + L_1^2 m_r)(m_r + m_p)} \end{cases} \tag{15}$$

where, $\dot{\varphi}$, $\ddot{\varphi}$, $\dot{z}_p$ and $\ddot{z}_p$ are the first and second derivatives of the connecting rod angle and piston displacement with respect to time, respectively; L_1 is the distance from the center of the small end bearing shell to the center of mass; m_r and m_p are the masses of the connecting rod and the piston, respectively; I_r is the moment of inertia of the connecting rod, and L_c is the the length of the rod; F_g is the resultant force of the combustion pressure acting on the piston.

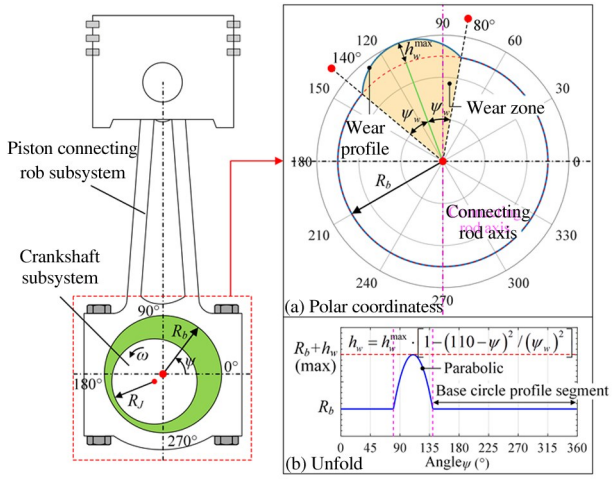

Fig. 2 Schematic diagram of subsystem and local wear profile of connecting rod bearing

2.2 Crankshaft subsystem

According to the torque balance principle of the crankshaft, the dynamic equation of the crankshaft subsystem can be expressed as

$$I_c\ddot{\theta} = F_{xc}R\cos\theta + F_{zc}R\sin\theta + T_f + T_l + T_p \tag{16}$$

$$T_f = 0.697\frac{\dot{\theta}}{|\dot{\theta}|} + \dot{\theta}(2.995\times10^{-8}\times n_c - 1.487\times10^{-5})V_c \tag{17}$$

where, I_c is the moment of inertia of the crankshaft system, F_{xc} and F_{zc} are the component of the bearing force of the big end bearing shell, T_l is the load torque, T_p is the driving torque of the remaining cylinders to the crankshaft, T_f is the frictional resistance torque of the system, $n_c = 4$ is the number of cylinders.

3 Simulation analysis of lubrication and wear impact characteristics

3.1 Simulation settings

On the basis of the above model, the simulation research on the lubrication and wear impact characteristics of connecting rod bearing bush is further carried out.

According to the actual bearing wear characteristics, two wear fault states are set: overall wear and local wear. In the overall wear state, the bearing clearance $c = 0.4$ mm. Fig. 2 is a schematic diagram of the local wear profile of the local wear state, with reference to the existing research experience, the wear interval span is set at 60 °, located in the upper half of the tile with the connecting rod axis as the boundary, and the rotation direction along the journal, the first 10 ° is the starting point, and the last 50 ° is the end point.

Fig. 1 shows the contour of the local wear of the big end bearing shell. Assuming that the wear profile ψ is parabolic (symmetric) relative to the rotation angle, the maximum wear depth is set to $h_w^{\max} = 12$ μm, so the wear profile can be expressed as

$$h_w = h_w^{\max}\left[1 - \frac{(110 - \psi^2)}{\psi_w^2}\right] \tag{18}$$

where $\psi_w = 30$ ° is the half wrap angle of the wear profile.

The specific simulation parameters are shown in Table 1.

Table 1 Specific settings of initial parameters in the simulation model

Characteristic parameter	Numerical value
Crank shaft moment of inertia (I_c)	0.1 kg · m^2
Connecting rod moment of inertia (I_r)	0.002 kg · m^2
Piston mass (m_p)	0.467 kg
Connecting rod mass (m_r)	0.693 kg
Crank angle (θ)	0 rad
Crank shaft angular velocity ($\dot{\theta}$)	210 rad/s
Connecting rod angle (φ)	π
Crank radius (R)	0.043 m
Connecting rod length (L_c)	0.135 m
The length from the small end of the connecting rod to the center of mass (L_1)	0.09 m
Cylinder volume (V_c)	0.000 47 m^3
Connecting rod angular velocity ($\dot{\varphi}$)	−66.9 rad/s
The position of the piston in the z direction (z_p)	0.177 997 m
The velocity of the piston in the z direction ($\dot{z}_p$)	0 m/s

3.2 Analysis of simulation results of oil film support force

The simulation sets the normal condition with a gap $c = 0.1$ mm and three fault conditions with $c = 0.2$ mm, $c = 0.3$ mm and $c = 0.4$ mm. For visual comparison, the normal condition and the uniform wear condition with a gap value of 0.4 mm are chosen to show the characteristic values. The simulation results of the overall wear of the bearing bush are shown in Fig. 3, and the oil film force of the big end bearing shell under normal conditions is used for comparison. It can be seen that with the occurrence of wear, the bearing bush clearance increases, and the peak oil film pressure in the wear state has a hysteresis characteristic compared with the normal state; after the overall wear, in the compression stroke before the diesel engine fires and the first bottom dead center (BDC) position after the fire, the high frequency impact force characteristic is generated, and the impact energy and range at the bottom dead center position are relatively large. The characteristic curves of the gap value 0.2 mm and 0.3 mm also have the same pattern.

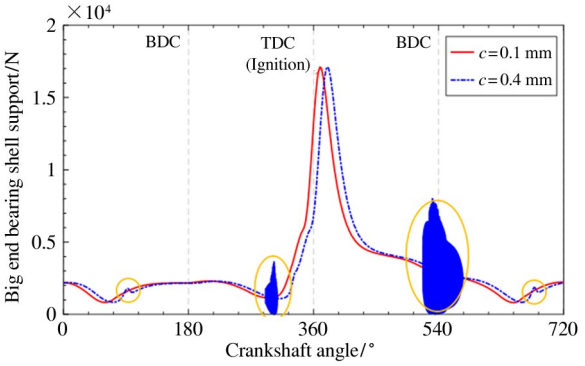

Fig. 3 Comparison of oil film resultant force of big end bearing shell under overall wear and normal state

However, the actual fault inspection and maintenance found that the overall uniform wear of the connecting rod bearing bushes is not a common wear state. Most engineering cases have proved that the big end bearing shell often wears unevenly, and the local wear is serious. The common wear area is the oil film during the ignition process. This is the area where the pressure is mainly applied. Fig. 4 shows the oil film force curve for a normal condition with a gap value of $c = 0.1$ mm and a wear condition with a maximum local wear depth of 0.4 mm. As shown in the figure, when the bearing bush is partially worn, at the two BDC positions of a single working cycle (720°) of the diesel engine the strong high-frequency impact force is generated; moreover, at the top stop of the non-firing stroke, a small shock is also produced near the 45° before and after the point. The characteristic curves of the gap value 0.2 mm and 0.3 mm also have the same pattern.

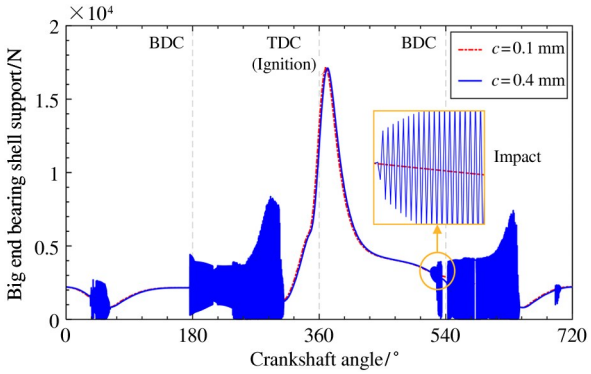

Fig. 4 Comparison of oil film forces of big end bearing shell under local wear and normal conditions

In order to better compare the oil film force variation law under the variable clearance condition, Fig. 5 further shows some indicators of the oil film force for the deepest local wear of $c = 0.1$ mm, 0.2 mm, 0.3 mm and 0.4 mm for a more realistic local wear condition. In Fig. 5, Impact 1 is the impact near the first BDC, i.e., the angle range of 170° – 306°; Impact 2 is the impact near the second BDC, i.e., the angle range of 520° – 648°. The maximum peak and root mean square (RMS) values of the shocks in these two angular domains are extracted separately, and the four curves in Fig. 5 are obtained. In this case, 20 cycles are set for each working condition, and the peak and RMS values are the average of the 20 cycles. It can be found that as the gap increases, the impact in the impact angle domain becomes more and more severe, in both Impact 1 and Impact 2.

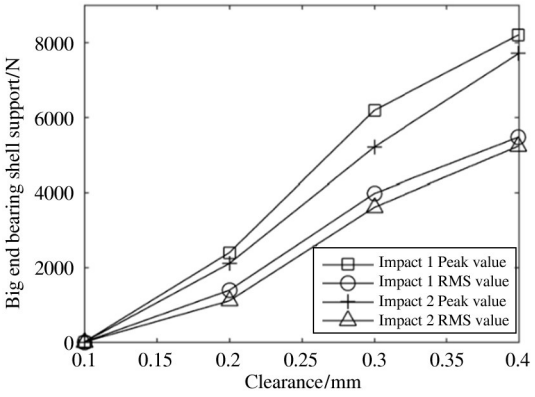

Fig. 5 The peak value and RMS value of the support force

3.3 Vibration acceleration signal analysis

On the basis of the above oil film force simulation results, the vibration acceleration signal of diesel en-

gine shell is further simulated. The frequency response function (FRF), which is excited and transmitted from the crank journal to the outer surface of the casing, is used to transform the supporting force of the big end bearing shell into the vibration acceleration signal of the engine casing, so that the vibration characteristics can be monitored and analyzed more directly. Fig. 6 shows the frequency response function from crank journal of piston engine to the position of main bearing on the surface of engine block. It can be seen from this figure that the transmission effect of high-frequency impact components on the vibration transmission path is good, but the transmission rate of low-frequency components below 1000 Hz is low. The oil film force data of the big end bearing shell calculated in the previous article is transformed by fast Fourier transform, the amplitude-frequency signal is multiplied by this transfer function, and combined with the phase-frequency signal, it is transformed into the vibration acceleration waveform of the machine body surface by inverse Fourier transform. The acceleration simulation signal in normal state is shown in Fig. 7, and the acceleration simulation signal in fault state is shown in Fig. 8 and Fig. 9. For the sake of visual comparison, only the wear gap of 0.4 mm is shown here, and the variation of vibration acceleration with the gap value is further illustrated in Fig. 10.

As can be seen from Fig. 6, under normal conditions, in a single working cycle of diesel engine, the oil film force of bearing bush changes smoothly, and the amplitude of acceleration impact is small, not exceeding 100 m/s^2.

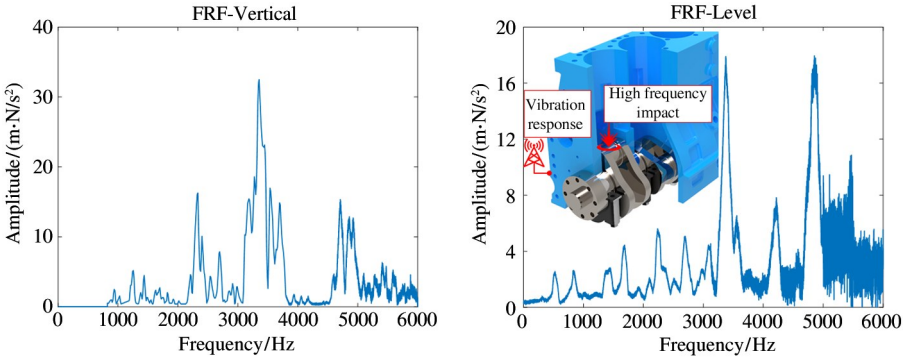

Fig. 6 Frequency response function of engine crank to shell surface

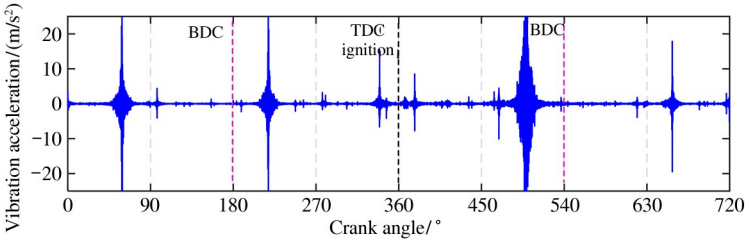

Fig. 7 Acceleration simulation signal in normal state

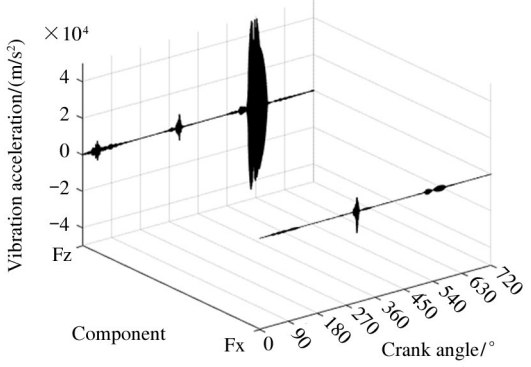

Fig. 8 The vibration signal of the body in response to the combined force of the oil film in the overall wear condition

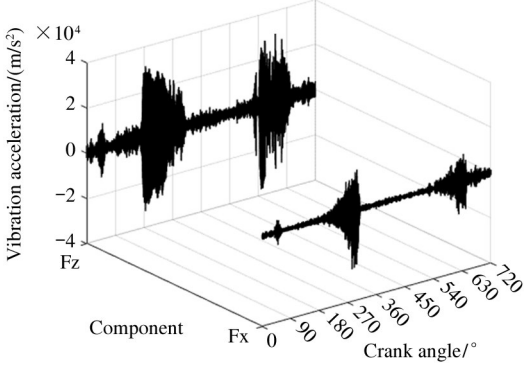

Fig. 9 The vibration signal of the body in response to the combined force of the oil film in the local wear condition

Further, the acceleration vibration signal under the condition of overall wear and local wear is simulated and analyzed.

Fig. 8 shows the vibration simulation signal generated by the oil film pressure under the overall wear condition. It can be seen that at the BDC phase after ignition, a significant vibration impact signal is generated, with a peak value of 4.8×104 m/s^2; there are also small vibration impacts around 45 ° and 300 °. Fig. 9 shows the vibration simulation signal generated by oil film pressure under local wear condition. It can be seen that significant vibration impact signals are generated at two BDCs before and after ignition, and the peak value is as high as 3.6×104 m/s^2. Compared with the overall wear condition, vibration impact is also generated at the BDCs before ignition. These vibrational shocks correspond to the abnormal phase of the oil film forces. The characteristic curves of the gap value 0.2 mm and 0.3 mm also have the same pattern.

In order to further compare the variation law of vibration acceleration under variable clearance, for the four gap values, the peak and RMS values of the impact near the first BDC (Impact 1 with an angular domain of 170 ° – 306 °) and the second BDC (Impact 2 with an angular domain of 520 ° – 648 °) are extracted, as shown in Fig. 10. And these values are obtained by averaging the results over 20 cycles. It can be found that as the gap value increases, the impact amplitude and the RMS value increases synchronously.

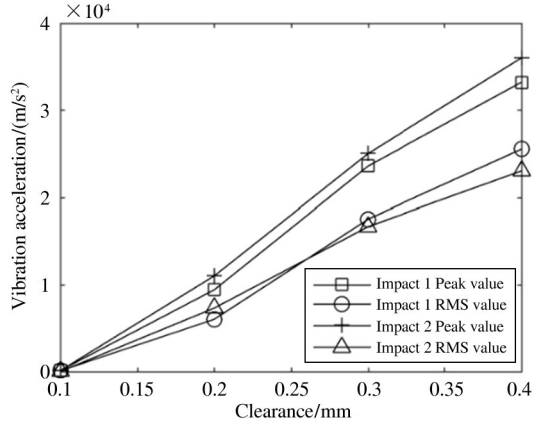

Fig. 10 The peak value and RMS value of the vibration acceleration

4 Results analysis and experimental verification

4.1 Experimental equipment and preparation

The vibration and impact characteristics of bearing shell after wear under ideal conditions are obtained from the above simulative results. Experimental verification research is further carried out. The experimental platform of this paper is shown in Fig. 11 and Table 2.

Fig. 11 Diesel engine fault simulation test bench

Table 2 Specific parameters of diesel engine test bench

Parameters	Value
Number of cylinders	12
Firing sequence	B1-A1-B5-A5-B3-A3-B6-A6-B2-A2-B4-A4-A1
Rated power	485 kW
Angle of cylinder	V-60 °
Rated speed	2100 r/min
Theoretical value of inlet valve clearance	0.3 mm

4.2 Experimental signal verification analysis

The wear fault simulation experiment of connecting rod's big end bearing shell of diesel engine is carried out. Taking A3 cylinder as the object, the connecting rod big end bearing bush is injected with fault injection method to manufacture part wear fault manually. The wear part was processed on the inner surface of the big end bearing shell by wire electrical discharge technology, and the part wear contour was formed. The part wear interval span is 60 °, the distribution position is the same as that in the simulation case, four working conditions with maximum wear depth of 0.1 mm, 0.2 mm, 0.3 mm and 0.4 mm are set respectively, and the wear contour is parabolic (symmetrical distribution). The details are shown in Fig. 12. The thickness of the alloy layer of the connecting rod's big end bearing shell is about 0.4 mm, and the maximum wear depth has reached the steel back layer. Therefore, this paper sets a relatively serious wear fault.

Install the acceleration vibration sensor on the lower surface of the crankshaft main bearing seat and drill the cable out of the oil pan. Considering the complex structure and working conditions of diesel engine, there are many vibration excitation sources, and the vibration signal on the surface of the body is usually interfered by strong noise, so the installation position of the sensor is as close to the connecting rod bearing shell

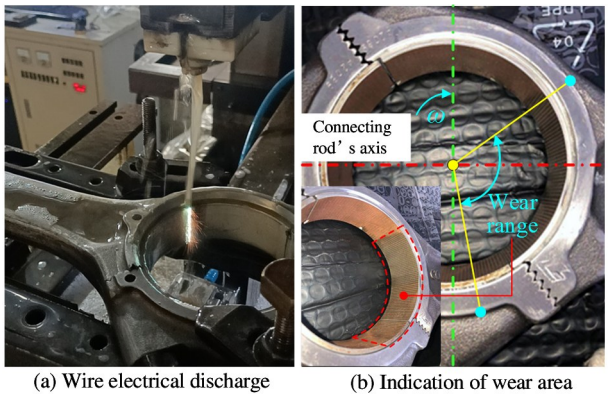

(a) Wire electrical discharge (b) Indication of wear area

Fig. 12 Diagram of the fault setting for partial wear of the big head of the connecting rod

as possible. The normal bearing and the faulty bearing are respectively used for the experiment. The experiment process is that the normal bearing is used first, and the engine is run at 1000 r/min and 400 N · m for 4 min; The data collector is used to collect data synchronously from the vibration sensor at a sampling frequency of 25.6 kHz. Then, the machine is shut down to disassemble and replace the partially severely worn big end bearing shell, and the experiments are conducted under the same working condition.

Fig. 13 shows the comparison of vibration waveform and spectrum collected by acceleration vibration sensor under normal and $c = 0.4$ mm wear conditions, with only one set of wear conditions selected to show the ease of observation. According to the firing sequence of the diesel engine, the top dead center of the A3 cylinder is located at 330 °, and the two bottom dead center are located at 150 ° and 510 ° respectively. It can be seen from the figure that the wear fault leads to significant vibration impact of the phases of the two bottom dead center. Moreover, the frequency of the impact component is distributed in the high frequency range of 10 – 15 kHz.

The waveforms and frequency domain plots for local maximum wear of $c = 0.2$ mm and $c = 0.3$ mm also show the same pattern. To further investigate the variation pattern of the vibration eigenvalues, 15 sets of experimental results for each clearance condition are shown in Fig. 14 and Fig. 15. In the time-domain plot of the vibration acceleration, the peak values of Impact 1

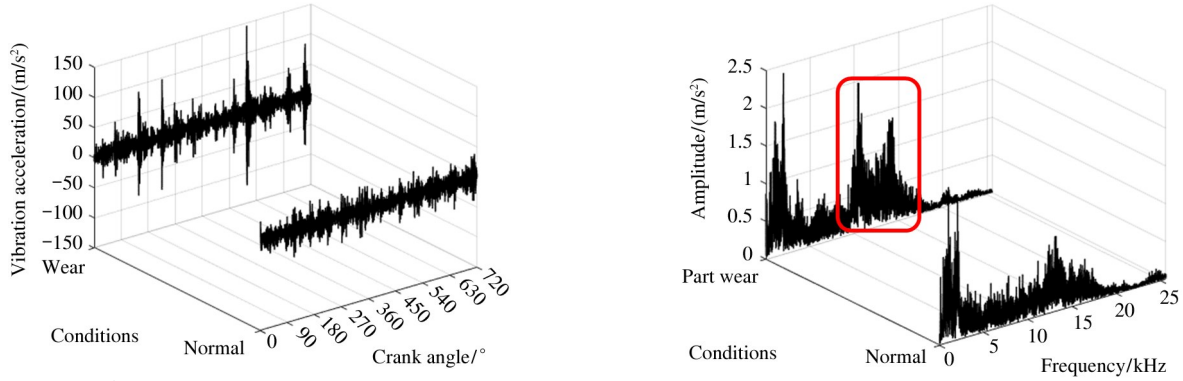

(a) Vibration acceleration waveform (b) Vibration spectrum

Fig. 13 Comparison of vibration waveforms and spectra under normal and wear conditions

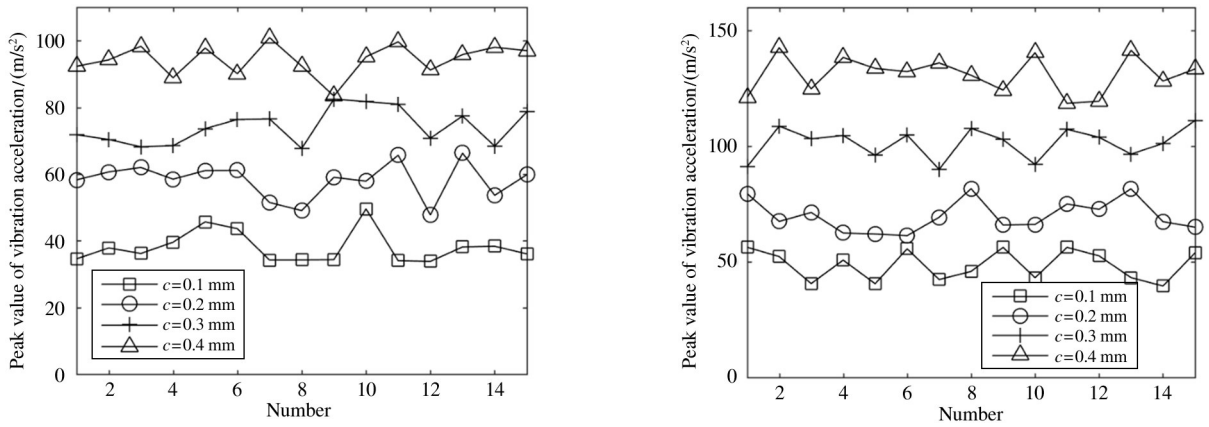

(a) Peak value of Impact 1 in the time domain waveform (b) Peak value of Impact 2 in the time domain waveform

Fig. 14 Peak values of vibration acceleration in the time domain waveform

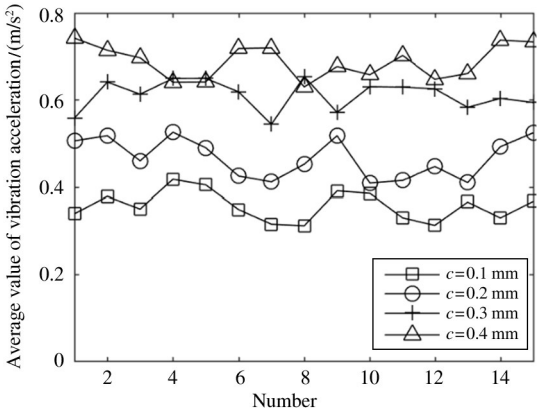

Fig. 15 Average value of vibration acceleration in the spectrogram

in the angular domain near the first BDC (i.e., 140° −160°) and Impact 2 in the angular domain near the second BDC (i.e., 500° −520°) are extracted to obtain Fig. 14. It can be found that the amplitude of shocks appearing in the angular domain near the two BDCs gradually increases as the gap value increases. In the frequency domain plot of the vibration acceleration, the average value in the frequency domain of 10 −15 kHz is extracted to obtain Fig. 15. It can be seen that the vibration eigenvalues fluctuate periodically at the same gap, but the vibration degree increases significantly with the increase of the gap value.

In conclusion, the experimental data of fault simulation verify the correctness of the simulation results of wear fault mechanism of connecting rod's big end bearing shell of diesel engine.

5 Conclusions

In order to solve the problems such as high fault rate, unclear fault mechanism and characteristics, and difficult diagnosis of connecting rod's bearing shell of diesel engine in the actual operation, a new full lubrication state analysis model of connecting rod's big end bearing shell is established, including full film lubrication, dry friction and a new mixed lubrication model considering the influence of material deformation. Coupled with the dynamics equation, the simulation of oil film force and shell acceleration is completed, and the ideal wear fault characteristics are obtained. The bearing shell's wear fault simulation experiment is carried out based on the diesel engine fault simulation test platform to verify the correctness of the theoretical research results.

This paper studies the impact of the connecting rod's bearing wear after important patterns and draws a conclusion that the pistons have significantly impact on the reversing point location signal. The research can be applied in the actual fault diagnosis of diesel engine, which has an important role in improving the accuracy of fault diagnosis of diesel engine and avoiding the occurrence of malignant faults such as the fracture of connecting rod and connecting rod's bolt.

References

[1] KE Y, SONG E Z, YAO C, et al. A review: ship diesel engine prognostics and health management technology [J]. Journal of Harbin Engineering University, 2020, 41 (1): 125-131. (In Chinese)

[2] PENG C. Fault analysis and preventive measures of connecting rod bolt of marine diesel engine[J]. Journal of Guangzhou Maritime Institute, 2016, 24(4): 14-15. (In Chinese)

[3] SUN L G, CHEN S, XIONG G. Fault analysis of aonnecting rod of diesel engine[J]. Diesel Engine, 2016, 38(6): 51-54. (In Chinese)

[4] DANIEL G B, CAVALCA K L. Analysis of the dynamics of a slider-crank mechanism with hydrodynamic lubrication in the connecting rod-slider joint clearance [J]. Mechanism and Machine Theory, 2011, 46 (10): 1434-1452.

[5] CHEN J, RANADALL R B. Intelligent diagnosis of bearing knock faults in internal combustion engines using vibration simulation[J]. Mechanism and Machine Theory, 2016,104: 161-176.

[6] HANEEF M D, RANDALL R B, SMITH W A, et al. Vibration and wear prediction analysis of IC engine bearings by numerical simulation[J]. Wear, 2017, 384: 15-27.

[7] HOU J X, DU J T. Vibration analysis of diesel engine body based on multi-body dynamics[C]// Proceedings of the 13th National Conference on Vibration Theory and Application. Xi'an: ICOVP, 2019: 373-377.

[8] YUAN Y B, WANG Z Y, WANG D H, et al. Failure investigation of a marine diesel engine timing gear[J]. Engineering Failure Analysis, 2020, 107: 1-13.

[9] BI F R, LIU B, LIU C C, et al. Research on diesel engine connecting rod small end bearing lubrication based on thermal elastic hydrodynamic model[J]. Chinese Internal Combustion Engine Engineering, 2018, 39 (4): 15-22. (In Chinese)

[10] SCARAGGI M, PERSSON B N J. Theory of viscoelastic lubrication[J]. Tribology International, 2014, 72: 118-130.

[11] HABCHI W, DEMIRCI I, EYHERAMENDY D, et al. A finite element approach of thin film lubrication in circular EHD contacts [J]. Tribology International, 2007, 40 (10): 1466-1473.

[12] PUTIGNANO C, AFFERRANTE L, CARBONE G, et al. Journal of the mechanics and physics of solids the influence of the statistical properties of self-affine surfaces in

elastic contacts: a numerical investigation[J]. Journal of the Mechanics and Physics of Solids, 2012, 60: 973-982.

[13] HE T, WANG Q J, ZHANG X, et al. Modeling thermal-visco-elastohydrodynamic lubrication (TVEHL) interfaces of polymer-based materials[J]. Tribology International, 2021,154(8): 1-15.

[14] WANG Z J, ZHANG J J, JIANG Z N, et al. A transient and time lag deformation alternating-coupling micro elastohydrodynamic lubrication model[J]. International Journal of Mechanical Sciences, 2021, 210: 1-18.

[15] PATIR N, CHENG H S. An average flow model for determining effects of three-dimensional roughness on partial hydrodynamic lubrication [J]. Journal of Tribology, 1979,100(1): 12-17.

[16] OCVIRK F. Short-bearing approximation for full journal bearings: NACA-TN-2808 [R]. Washington: NACA, 1952.

[17] LANKARANI H M, NIKRAVESH P E. A contact force model with hysteresis damping for impact analysis of multibody systems [J]. Journal of Mechanical Design, 1990,112(3): 369-376.

[18] FLORES P. Modeling and simulation of wear in revolute clearance joints in multibody systems [J]. Mechanism and Machine Theory, 2009,44(6):1211-1222.

GAO Yunduan, born in 1986. She received her B. S. degree from Liren College, Yanshan University in 2009 and her M. S. degree from Beijing University of Technology in 2012. Her research mainly engaged in advanced sensor technology research.